

# Anamorphic Free-Form Deformation <sup>☆</sup>



Javier Sánchez-Reyes <sup>\*</sup>, Jesús M. Chacón

Universidad de Castilla-La Mancha, IMACI, ETS Ingenieros Industriales, Ciudad Real, Spain

## ARTICLE INFO

### Article history:

Received 12 December 2015

Received in revised form 11 June 2016

Accepted 13 June 2016

Available online 23 June 2016

### Keywords:

Anamorphosis

Free-Form Deformation

NURBS

Perspective collineation

Rational Bézier volume

Stereographic projection

## ABSTRACT

In an optical anamorphosis, an object is seen distorted unless the viewer is positioned at a specific point, where the object appears normal. We describe how to endow a rational Free-Form Deformation with an anamorphic character in a simple manner, obtaining an AFFD (Anamorphic Free-Form Deformation). Given a (planar or 3D) initial object, which will appear normal from the desired viewpoint, we deform the object with a rational Bézier surface or volume as deformation tool. To achieve the desired deformation, the user input amounts to displacing the control points of the deformation tool along radial directions through the viewpoint, whereas the weights come as a byproduct. Mathematically, the deformation means changing the last homogeneous coordinate of the control points. An AFFD defined by a linear Bézier tetrahedron can be regarded as a user-friendly way to construct a perspective collineation. In this case, or when the deformation tool is a Bézier triangle of degree one, the AFFD transforms NURBS to NURBS keeping the original degree. With a deformation tool of higher degree, the rational composition required to obtain the exact result yields NURBS also of higher degree. For a quadratic Bézier triangle as deformation tool, our AFFD coincides with the inverse of a stereographic projection.

© 2016 The Authors. Published by Elsevier B.V. This is an open access article under the CC BY-NC-ND license (<http://creativecommons.org/licenses/by-nc-nd/4.0/>).

## 1. Introduction

### 1.1. Anamorphic images

*Anamorphic images* are those that appear distorted unless viewed from a particular viewpoint (*optical* anamorphosis) or with a suitable mirror or lens (*catoptric* anamorphosis). In this article, we focus on optical anamorphosis, requiring no optical device for a correct view.

A typical optical anamorphosis is shown in Fig. 1, where a logo  $\hat{S}$  painted on a twisted surface appears distorted when observed from a general viewpoint, such as that used in this illustration, but becomes recognizable, seen as the undistorted logo  $S$ , if the observer is located at a certain point  $O$ . Another remarkable effect could be achieved when the initial object  $S$  is a picture of a 3D object taken from  $O$ . Then, an observer at  $O$  easily mistakes  $\hat{S}$  for the 3D object. This is the technique behind anamorphic pavement drawings, such as those designed by Beaver (2012), or the 3D illusion of anamorphic frescos painted on vaults by classical painters. Many examples and applications in architecture can be found in the recent article by Di Paola et al. (2015). An optical anamorphosis is also possible by deforming 3D geometry, such as the Stanford bunny

<sup>☆</sup> This paper has been recommended for acceptance by Gerald Farin.

<sup>\*</sup> Corresponding author.

E-mail address: [Javier.SanchezReyes@uclm.es](mailto:Javier.SanchezReyes@uclm.es) (J. Sánchez-Reyes).

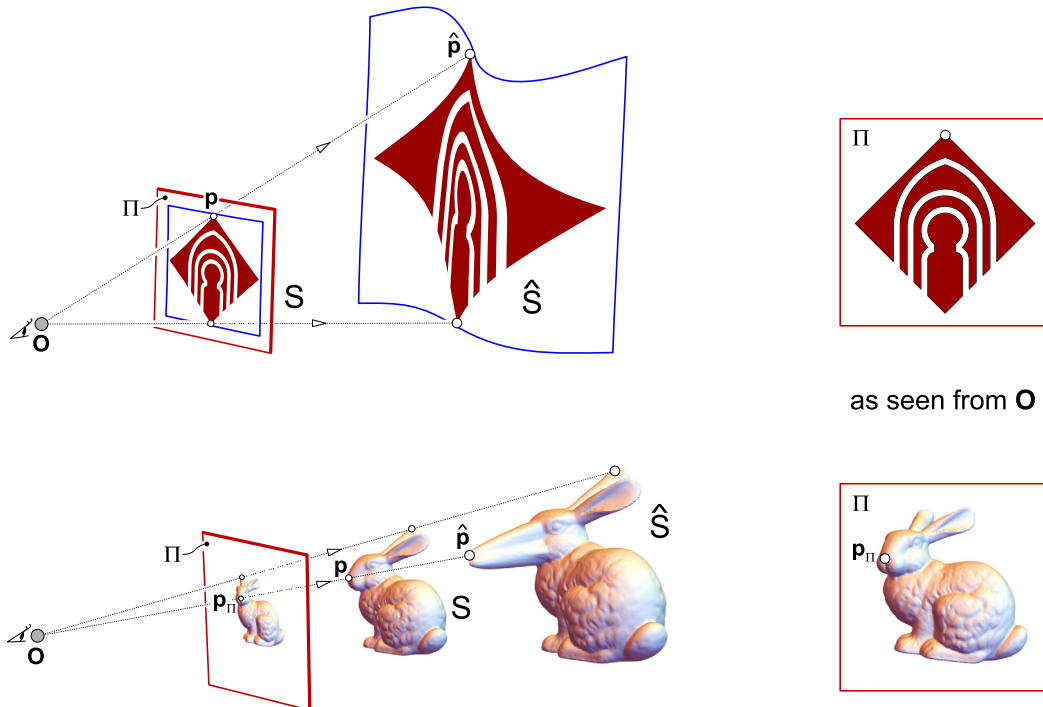


Fig. 1. Anamorphic versions  $\hat{S}$  of a planar logo and a 3D bunny  $S$ .

(Stanford Computer Graphics Laboratory, 2014) of Fig. 1. A viewer sees a distorted 3D object  $\hat{S}$  from  $O$  and mistakes it for a more familiar (undistorted) version  $S$ , to realize the true shape of  $\hat{S}$  after moving away from  $O$ .

Anamorphosis is hardly mentioned in traditional textbooks on Computer Graphics, only receiving some attention in two manuals by Salomon (2006, 2011). However, this fascinating technique has been employed by artists and architects for centuries, as illustrated in the webpage by Kent (2013), and has also drawn the attention of researches on visual perception (Topper, 2000). Anamorphosis is utilized for visual effects in popular TV series, such as Brain Games (National Geographic Channel, 2015), or video games (FDG Entertainment, 2015). An anamorphosis can even be dynamic, adapting itself to a changing position of the observer, which finds applications to improve eye contact in videoconferencing (Ravnik et al., 2014).

### 1.2. Anamorphosis as a radial deformation

The basic mathematics behind an optical anamorphosis are surprisingly simple, something not always made clear in the existing literature. Given a viewpoint  $O$ , where the observer is located, and an initial object  $S$ , to generate an anamorphic version  $\hat{S}$  just deform  $S$ , by displacing each point  $p$  on the object to a new position  $\hat{p}$  along a radial line through  $O$ , as shown in Fig. 1. In consequence, given an arbitrary view plane  $\Pi$  where objects are projected,  $p$  and  $\hat{p}$  have exactly the same perspective projection  $p_\Pi$  with center  $O$ . Thus,  $S$  and  $\hat{S}$  share a common silhouette and their edges have the same projection, so in a traditional non-photorealistic line drawing (silhouettes and edges), or in a wireframe representation, the two objects appear identical. If  $O$  lies at infinity, the perspective projection degenerates to parallel and the anamorphic radial deformation transforms to what Elber (2011) calls *Line of Sight Deformation*, in his work for modeling seemingly impossible objects.

In a shaded or photorealistic rendering, or with real objects, the renderings of  $S$  and  $\hat{S}$  would not be identical. Indeed, nor the points  $p, \hat{p}$  neither their corresponding normals coincide, hence reflecting the incoming light in a different way. However, both objects would be difficult to distinguish from each other, in particular if they are textured. The projection of textures is not affected by the anamorphosis, which mitigates the lighting problem and enhances the deception effect. Anamorphic objects are thus *appearance-mimicking*, a term coined by Schüller et al. (2014) to characterize bas-reliefs and other surfaces that look similar to another one from a fixed viewpoint while having different geometry. Whereas in a general anamorphosis the points move freely along radial directions, Schüller et al. (2014) design a thin surface, i.e., with a narrow depth range, trying to preserve the surface normals in order to minimize the visual difference under a diversity of illumination conditions. More information on computer-assisted relief generation is found in the survey (Kerber et al., 2012) and references therein, including the work (Bian and Hu, 2011) on preservation of detailed features.

### 1.3. Anamorphosis via FFD (Free-Form Deformation)

Rather than a tedious point-by-point anamorphic deformation of the initial object, a more sensible alternative is clearly the use of some FFD (Free-Form Deformation) technique, a term coined by Sederberg and Parry (1986). Indeed, for creating anamorphic 3D geometry, Hansford and Collins (2007) advocate the use of a *collineation*, a certain linear map in projective space that can be regarded as a rational linear FFD. Sela and Elber (2007) also employ a FFD (in this case, a polynomial B-spline FFD) to generate deceiving geometry. However, instead of an anamorphosis, their goal is to merge two 3D objects into a common geometry, which resembles the first object from one viewing direction and the second one from another orthogonal direction. In our work, following the initial ideas by Hansford and Collins (2007), we develop more general anamorphic transformations for true perspective projection, in terms of a rational FFD. Thus, we give a modern interpretation of anamorphosis, more accessible for implementation in CAGD and a NURBS setting.

The paper is arranged as follows. First, in Section 2, we note that the key idea to simplify the mathematics behind anamorphosis is the use of homogeneous coordinates, with origin at the center  $\mathbf{O}$  of perspective. Then, in Section 3 we tackle the initial case of the anamorphic deformation of a planar object, using an embedding rational surface as deformation tool. The underlying mathematics carry over easily to the deformation of 3D geometry using a rational volume (Section 4). Finally, conclusions and extensions of this work are outlined in Section 5.

## 2. Anamorphosis made simple: homogeneous coordinates

### 2.1. Homogeneous coordinates

In this section, we recall that an optical anamorphic transformation becomes trivial in homogeneous coordinates, with origin at the center  $\mathbf{O}$  of perspective. First, some remarks regarding terminology and notation. Given an *affine* point  $\mathbf{p}$  in *Euclidean* 3D-space, its *homogeneous* counterpart  $\underline{\mathbf{p}}$  in *projective* space is generating by adding a forth unit coordinate (and optionally multiplying by a nonnegative scalar *weight*  $w$ ):

$$\mathbf{p} = \begin{Bmatrix} x \\ y \\ z \end{Bmatrix}, \quad \underline{\mathbf{p}} = w \begin{Bmatrix} \mathbf{p} \\ 1 \end{Bmatrix}, \quad w \neq 0. \quad (1)$$

Adhering to the notation introduced by Farin (1999), homogeneous points  $\underline{\mathbf{p}}$  will be underlined to distinguish them from their affine counterparts  $\mathbf{p}$ . The projection mapping  $\underline{\mathbf{p}}$  back to Euclidean space amounts to dividing the first three coordinates by the forth one and dropping the latter.

Let us apply a deformation  $\Phi$ , yielding a new point  $\hat{\mathbf{p}} = \Phi(\underline{\mathbf{p}})$ , such that only the last component of  $\mathbf{p}$  changes:

$$\underline{\mathbf{p}} = w \begin{Bmatrix} \mathbf{p} \\ 1 \end{Bmatrix} \xrightarrow{\Phi} \hat{\underline{\mathbf{p}}} = w \begin{Bmatrix} \mathbf{p} \\ \delta \end{Bmatrix} \rightarrow \hat{\mathbf{p}} = \mathbf{p}/\delta. \quad (2)$$

The new affine point  $\hat{\mathbf{p}}$  is simply a scaled version (with center  $\mathbf{O}$  and dilation factor  $1/\delta$ ) of the original  $\mathbf{p}$ , that is,  $\hat{\mathbf{p}}$  lies on the radial line  $\mathbf{Op}$ . Therefore, its projection  $\mathbf{p}_\Pi$  on any given view plane  $\Pi$  remains unchanged. As remarked by Farin (1999), all points on the line  $\mathbf{Op}$ , being indistinguishable for the observer, are equivalent in projective geometry. Thus, by applying the transformation (2) to all points of an object  $S$ , we generate an anamorphic sibling  $\hat{S}$ .

### 2.2. NURBS curves and surfaces

If the object is defined using a boundary representation (B-rep), with NURBS curves or surfaces (Farin, 1999; Piegl and Tiller, 1997), we can rather apply the anamorphic dilation to the NURBS control points, instead of point-by-point.

Consider a NURBS curve  $\mathbf{p}(t)$ , over a certain knot vector, with homogeneous control points  $\underline{\mathbf{p}}_i$  or, equivalently, affine points  $\mathbf{p}_i$  and weights  $w_i$ . Now, let us modify only the last homogeneous component of  $\underline{\mathbf{p}}_i$ , as in (2). This operation  $\Phi$  yields another NURBS curve, over the same knot vector, with new points and weights  $\hat{w}_i$ :

$$\underline{\mathbf{p}}_i = w_i \begin{Bmatrix} \mathbf{p}_i \\ 1 \end{Bmatrix} \xrightarrow{\Phi} \hat{\underline{\mathbf{p}}}_i = w_i \begin{Bmatrix} \mathbf{p}_i \\ \delta_i \end{Bmatrix}, \quad \begin{matrix} \hat{\mathbf{p}}_i = \mathbf{p}_i/\delta_i \\ \hat{w}_i = w_i\delta_i \end{matrix}. \quad (3)$$

For each value of the parameter  $t$ , once again the new affine  $\hat{\mathbf{p}}(t)$  is obtained by dilating the original  $\mathbf{p}(t)$ , and thus  $\hat{\mathbf{p}}(t)$  amounts to an anamorphic version of  $\mathbf{p}(t)$ . Equivalently,  $\hat{\mathbf{p}}(t)$  lies on a cone with vertex  $\mathbf{O}$  and generatrix  $\mathbf{p}(t)$ . Though we are dealing with homogeneous coordinates, the user input amounts to choosing the desired final affine position  $\hat{\mathbf{p}}_i = \mathbf{p}_i/\delta_i$  along the radial direction  $\mathbf{Op}_i$ . The new weight  $\hat{w}_i = w_i\delta_i$  (3) associated to  $\hat{\mathbf{p}}_i$  comes as a by-product from  $\hat{\mathbf{p}}_i$ . In case  $\mathbf{p}_i = \mathbf{O}$ , then  $\mathbf{p}_i$  remains fixed and only its weight changes. More details on this NURBS modification technique are found in Sánchez-Reyes (1997).

Fig. 2 depicts a simple example, where the initial curve  $\mathbf{p}(t)$  is a circular arc segment, defined in quadratic rational Bézier form with three control points. This arc lies on the view plane  $\Pi$ , hence coinciding with the image seen by an observer

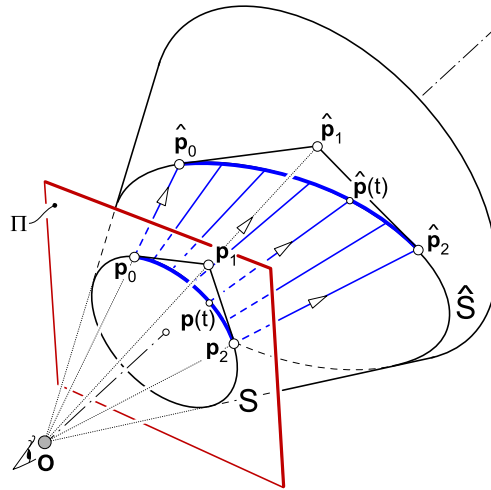


Fig. 2. Conic sections as anamorphic images  $\hat{S}$  of a circular arc  $S$ .

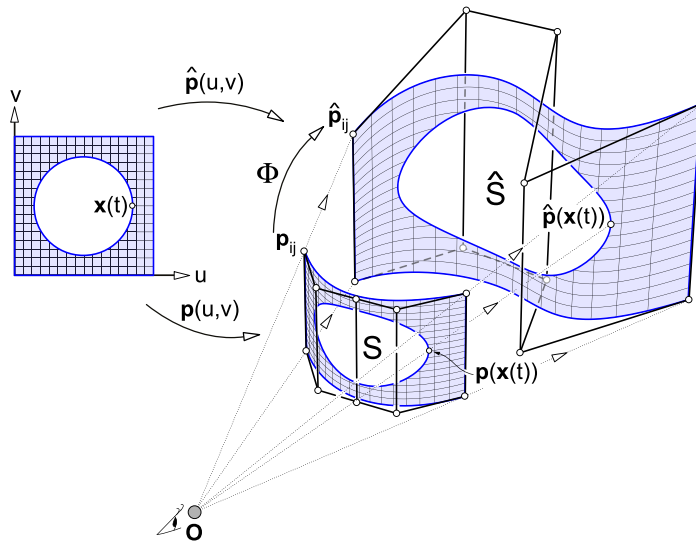


Fig. 3. Submitting a rectangular trimmed patch to an anamorphosis.

located at  $\mathbf{O}$ . If the control points are submitted to a transformation (3), the resulting planar curve  $\hat{\mathbf{p}}(t)$  lies on a circular cone, and we generate different conic sections. However, these sections are always perceived as a circle by an observer located at  $\mathbf{O}$ .

The extension to NURBS surfaces is a straightforward exercise: once again, simply apply transformation (3) to the control points. The case of trimmed patches (Farin and Hansford, 2000; Farin, 2002) deserves special attention for their widespread use in solid and surface modelers. In such patches certain areas are trimmed away by marking them as invalid, with *trimming curves* defined in the surface domain. Fig. 3 gives an example, a rectangular patch  $\mathbf{p}(u, v)$  with a trimming curve  $\mathbf{x}(t) = \{u(t), v(t)\}$  in the rectangular domain  $(u, v)$ . Remarkably, if we displace anamorphically (3) the control points of a NURBS trimmed patch  $S$ , keeping the original trimming curves in the domain, the resulting trimmed patch is an anamorphic image  $\hat{S}$  of  $S$ . Indeed, for each pair  $(u, v)$  the point  $\mathbf{p}(u, v)$  on  $S$  transforms anamorphically to  $\hat{\mathbf{p}}(u, v)$ , so in particular each point  $\mathbf{p}(\mathbf{x}(t))$  of the initial 3D trimming curve transforms anamorphically to the corresponding point  $\hat{\mathbf{p}}(\mathbf{x}(t))$  of the trimming curve on  $\hat{S}$ .

### 2.3. Anamorphic Free-Form Deformation (AFFD)

In the case of a complex object  $S$ , composed of several NURBS curves or patches, the manipulation of their individual control points would still be a tedious task. We can go a step further and employ instead a Free-Form Deformation. The idea is to embed the (planar or 3D) object  $S$  in a (planar or 3D) structure (i.e., a regular lattice of control points) and then deform

the structure by applying an anamorphic transformation to a lattice of control points  $\mathbf{b}_i$ . The resulting *Anamorphic Free-Form Deformation* (AFFD) propagates to  $S$ , yielding an anamorphic version  $\hat{S}$ . Next, we analyze the mathematics involved.

As in any FFD (Gain and Bechmann, 2008), given a point  $\mathbf{p}$  its image  $\hat{\mathbf{p}}$  stems from a two-step functional composition:

$$\mathbf{p} \xrightarrow{\mathbf{E}} \mathbf{u} \xrightarrow{\mathbf{d}} \hat{\mathbf{p}} \tag{4}$$

1. Find the local coordinates  $\mathbf{u}$  of  $\mathbf{p}$ , in the *local parameter space* associated to the deformation tool, before it is deformed, via an *embedding function*  $\mathbf{E}$  (basically, a change of coordinates).
2. Displace anamorphically the control points  $\mathbf{b}_i$  (with initial unit weights) to their new locations  $\hat{\mathbf{b}}_i$ , and compute  $\mathbf{d}(\mathbf{u})$  as:

$$\underline{\mathbf{b}}_i = \left\{ \begin{matrix} \mathbf{b}_i \\ 1 \end{matrix} \right\} \rightarrow \hat{\underline{\mathbf{b}}}_i = \left\{ \begin{matrix} \mathbf{b}_i \\ \delta_i \end{matrix} \right\}, \quad \hat{\mathbf{p}} = \mathbf{d}(\mathbf{u}) = \sum_i \hat{\underline{\mathbf{b}}}_i B_i(\mathbf{u}), \tag{5}$$

where the subscript  $i$  runs over the nodes of the lattice, and  $B_i(\mathbf{u})$  denotes the associated basis functions, forming a partition of unity.

If we do not move any  $\mathbf{b}_i$  the result of the composition (4) (in homogeneous version, with unit weight) coincides with the initial point  $\mathbf{p}$ . By dilating anamorphically the points  $\mathbf{b}_i$ , only the fourth component in  $\mathbf{d}(\mathbf{u})$  (5) is altered:

$$\underline{\mathbf{p}} = \left\{ \begin{matrix} \mathbf{p} \\ 1 \end{matrix} \right\} \xrightarrow{\Phi} \hat{\underline{\mathbf{p}}} = \mathbf{d}(\mathbf{u}) = \left\{ \begin{matrix} \mathbf{p} \\ \delta(\mathbf{u}) \end{matrix} \right\}, \quad \delta(\mathbf{u}) = \sum_i \delta_i B_i(\mathbf{u}), \tag{6}$$

which yields a functional version of transformation (2). Now, the scalar  $\delta$  (inverse of the dilation factor) is replaced with a dilation function  $\delta(\mathbf{u})$  depending on  $\mathbf{u}$ , in essence on the orientation of the ray  $\mathbf{Op}$ . If all points  $\mathbf{b}_i$  are dilated sharing a common  $\delta_i = \delta$ , the anamorphosis degenerates to a homogeneous dilation, with dilation factor  $1/\delta$ .

The user input amounts to moving the control points  $\mathbf{b}_i$  of the deformation tool along radial lines  $\mathbf{Ob}_i$ , to their desired final position  $\hat{\mathbf{b}}_i = \mathbf{b}_i/\delta_i$  in Euclidean space. The weight  $\hat{w}_i = \delta_i$  associated to  $\hat{\mathbf{b}}_i$  comes as a by-product. This AFFD allows hence the generation of anamorphic models in an intuitive way, since the user manipulates positions of affine points in Euclidean space.

### 3. AFFD of a planar object

In this section, we tackle the introductory case where a planar object  $S$  is submitted to an AFFD and transformed into an anamorphic sibling  $\hat{S}$ , not necessarily planar but embedded into a surface. The object  $S$  could be either a vector image (defined by lines and curves), or a bitmap image. We assume that  $S$  lies on the view plane  $\Pi$ , so that it coincides with the image seen by an observer located at the center  $\mathbf{O}$ .

In our AFFD, the user defines on  $\Pi$  a reference triangle  $T$  (or rectangle  $R$ ) embedding the object, and then chooses the degree of the deformation tool, which for the Bézier case results in a control mesh over  $T$  (or  $R$ ) with points evenly spaced. The homogeneous version of these points are assigned a unitary weight and finally the user displaces them anamorphically (5) away from  $\Pi$ , by choosing their final positions, to generate the desired anamorphic image  $\hat{S}$ .

#### 3.1. Rational linear AFFD

The simplest deformation tool is a triangular Bézier surface of degree  $n = 1$ , with three control points  $\mathbf{b}_0, \mathbf{b}_1, \mathbf{b}_2$ , corresponding to the vertices of a reference triangle  $T$  on  $\Pi$ . These points define a system of barycentric coordinates  $\mathbf{u} = (u_0, u_1, u_2)$  as local parameter space, where triplets  $\mathbf{u}$  with positive coordinates indicate the interior of  $T$ . The three points  $\mathbf{b}_i$  are assigned initially a unit weight, and then the user displaces them along radial directions  $\mathbf{Ob}_i$ , to their final positions  $\hat{\mathbf{b}}_i$ . This defines the new homogeneous points  $\hat{\underline{\mathbf{b}}}_i$  (5) and a rational linear deformation:

$$\mathbf{d}(\mathbf{u}) = \sum_{i=0}^2 u_i \hat{\underline{\mathbf{b}}}_i, \quad \underline{\mathbf{b}}_i = \left\{ \begin{matrix} \mathbf{b}_i \\ \delta_i \end{matrix} \right\}. \tag{7}$$

This geometry is shown in Fig. 4, where the initial object  $S$  is a letter. The first three components in (7) are inherited from the initial triangle (before deformation), and hence define the identity. Therefore, the AFFD indeed admits the compact form (6), where:

$$\delta(\mathbf{u}) = \sum_{i=0}^2 u_i \delta_i. \tag{8}$$

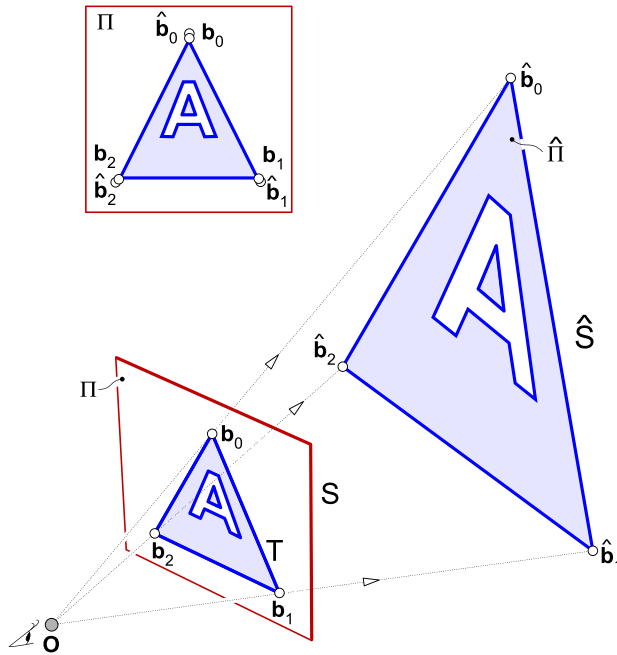


Fig. 4. Rational linear AFFD of a planar vector object, using a Bézier triangle.

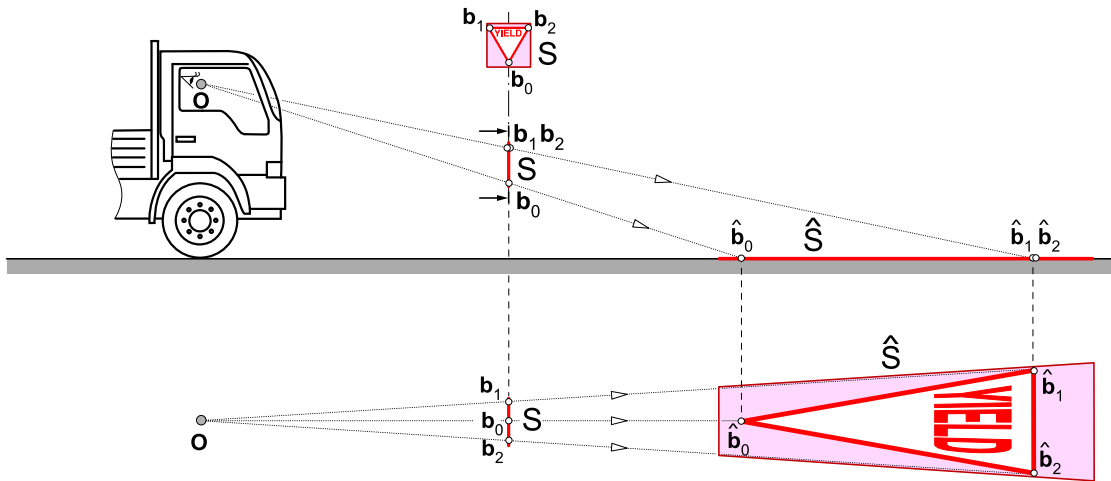


Fig. 5. Road marks as an example of rational linear AFFD.

This AFFD, being rational linear, amounts to a perspective projection with center  $\mathbf{O}$ , from the initial plane  $\Pi$  to the new plane  $\hat{\Pi}$  defined by  $\hat{\mathbf{b}}_0, \hat{\mathbf{b}}_1, \hat{\mathbf{b}}_2$ . As a consequence, lines project to lines, and to obtain the image of a line segment we simply find the image of its endpoints. Similarly, a NURBS curve  $\mathbf{p}(t)$  on  $\Pi$  of degree  $n$  transforms to another NURBS curve  $\hat{\mathbf{p}}(t)$  of the same degree, lying on  $\hat{\Pi}$ . Indeed, the AFFD  $\Phi$  is linear in homogeneous coordinates, so that  $\Phi(w\mathbf{p}) = w\Phi(\mathbf{p})$ . Therefore, a NURBS control point  $\mathbf{p}_k$  (with barycentric coordinates  $\mathbf{u}_k$  and weight  $w_k$ ) transforms as follows:

$$\underline{\mathbf{p}}_k = w_k \begin{Bmatrix} \mathbf{p}_k \\ 1 \end{Bmatrix} \xrightarrow{\Phi} \hat{\underline{\mathbf{p}}}_k = w_k \begin{Bmatrix} \mathbf{p}_k \\ \delta(\mathbf{u}_k) \end{Bmatrix}. \tag{9}$$

This rational linear anamorphosis is commonly seen in the symbols and drawings painted in the roads, as illustrated in Fig. 5: to replace a vertical traffic signal  $S$ , simply paint  $\hat{S}$  on the road. Whereas  $\hat{S}$  appears distorted when observed directly from above, this elongation compensates for the foreshortening perceived by an approaching driver.

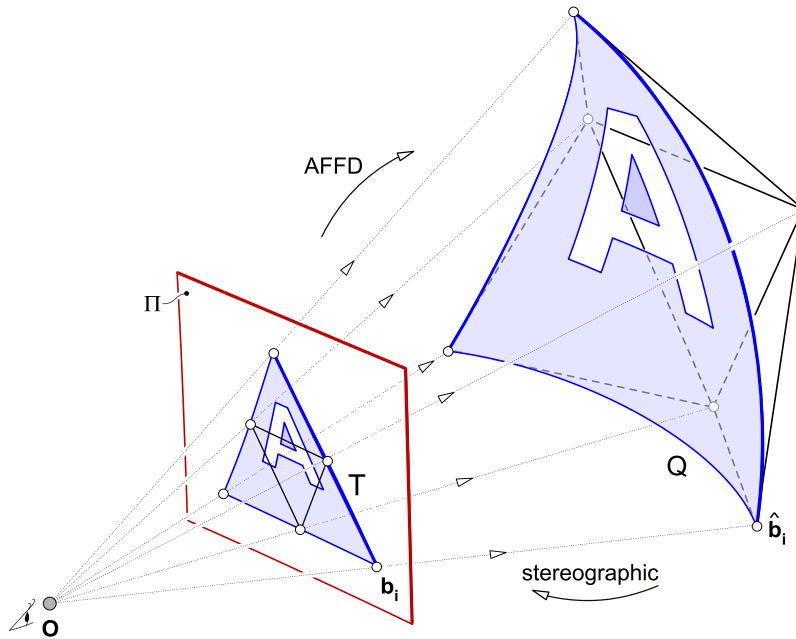


Fig. 6. Inverse of a stereographic projection as a rational quadratic AFFD.

### 3.2. Quadratic and higher-degree AFFD

The linear construction of Section 3.1 easily carries over to an AFFD with a triangular Bézier surface of arbitrary degree  $n$  as deformation tool. Next, we analyze the remarkable quadratic case ( $n = 2$ ). Now, the initial regular control mesh over the reference triangle  $T$  has 6 points (Fig. 6), with three new control points at the midpoints of the edges of  $T$ , resulting from standard degree-elevation of a linear Bézier triangle. These additional degrees of freedom allow the design of non-planar anamorphoses, but we could move all the points to a plane, recapturing the construction of Section 3.1.

Now, in the AFFD (6) the reciprocal  $\delta(\mathbf{u})$  of the dilation is quadratic, instead of linear (8). Therefore,  $T$  transforms into a rational quadratic Bézier patch  $Q$ . In general, such a patch lies on a quartic implicit surface called *Steiner surface* (Sederberg and Anderson, 1985). However, in this case the AFFD corresponds to the *canonical construction* of quadrics (Sánchez-Reyes and Paluszny, 2000), yielding a quadric  $Q$  through  $\mathbf{O}$  (when extended beyond the image of  $T$ ). In consequence, we are reproducing the inverse of a stereographic projection (Lodha and Warren, 1990; Boehm and Hansford, 1991; Teller and Séquin, 1991; Farin, 1999). This quadratic AFFD maps lines on  $\Pi$  to conics on  $Q$ , passing through  $\mathbf{O}$  when they are nondegenerate (i.e., different from a straight line). The celebrated stereographic projection, used in cartography, proceeds hence in opposite direction to the AFFD: we choose a point  $\mathbf{O}$  on the earth  $Q$  and then generate a map on a plane  $\Pi$  (parallel to the tangent plane at  $\mathbf{O}$ ), by firing rays from  $\mathbf{O}$ .

We can resort to a rectangular surface, instead of triangular, as deformation tool. Now, the user defines on  $\Pi$  a reference rectangle  $R$ . The embedding function  $\mathbf{E}$  (4) amounts to an affine map, mapping  $R$  to a unit square defining a local parameter space  $\mathbf{u} = (u, v) \in [0, 1] \times [0, 1]$ . Fig. 7a shows a simple example, a Bézier surface of degree (1, 1), with four control points  $\mathbf{b}_{00}, \mathbf{b}_{01}, \mathbf{b}_{10}, \mathbf{b}_{11}$  corresponding to the vertices of  $R$ . Any rational bilinear patch is a quadric, either a hyperbolic paraboloid or a hyperboloid of one sheet (Boehm and Hansford, 1991; Farin, 1999). Therefore, if we subdivide the rectangular domain into two subtriangles along a diagonal, at each triangle the AFFD yields the aforementioned inverse of a stereographic projection. A rectangular surface is clearly the tool of choice when the object  $S$  is a bitmap image (Fig. 7b), typically a rectangular pixel array. This AFFD admits a direct implementation using standard tools in graphic libraries, by adding a texture mapping  $S$  to the surface in parameter space. Observe that, as commented in Section 1.2, the projection of textures is not affected by the AFFD.

## 4. Volumetric AFFD of a 3D object

In this section, we study the case of a volumetric AFFD, where the object  $S$  to deform is 3D (instead of planar). The initial geometry  $S$  could be either an approximated faceted model, such as those employed for fast interactive rendering, or a more refined B-rep solid, with faces defined as NURBS patches.

First, the user embeds  $S$  in a 3D regular lattice of control points, used as a deformation tool. The homogeneous version of these points is assigned a unitary weight, so that initially the lattice induces a linearly parameterized hyperpatch. Then the user displaces the control points radially (5), to generate the desired anamorphic version  $\hat{S}$ . As a result, note two basic properties of the transformation (6):



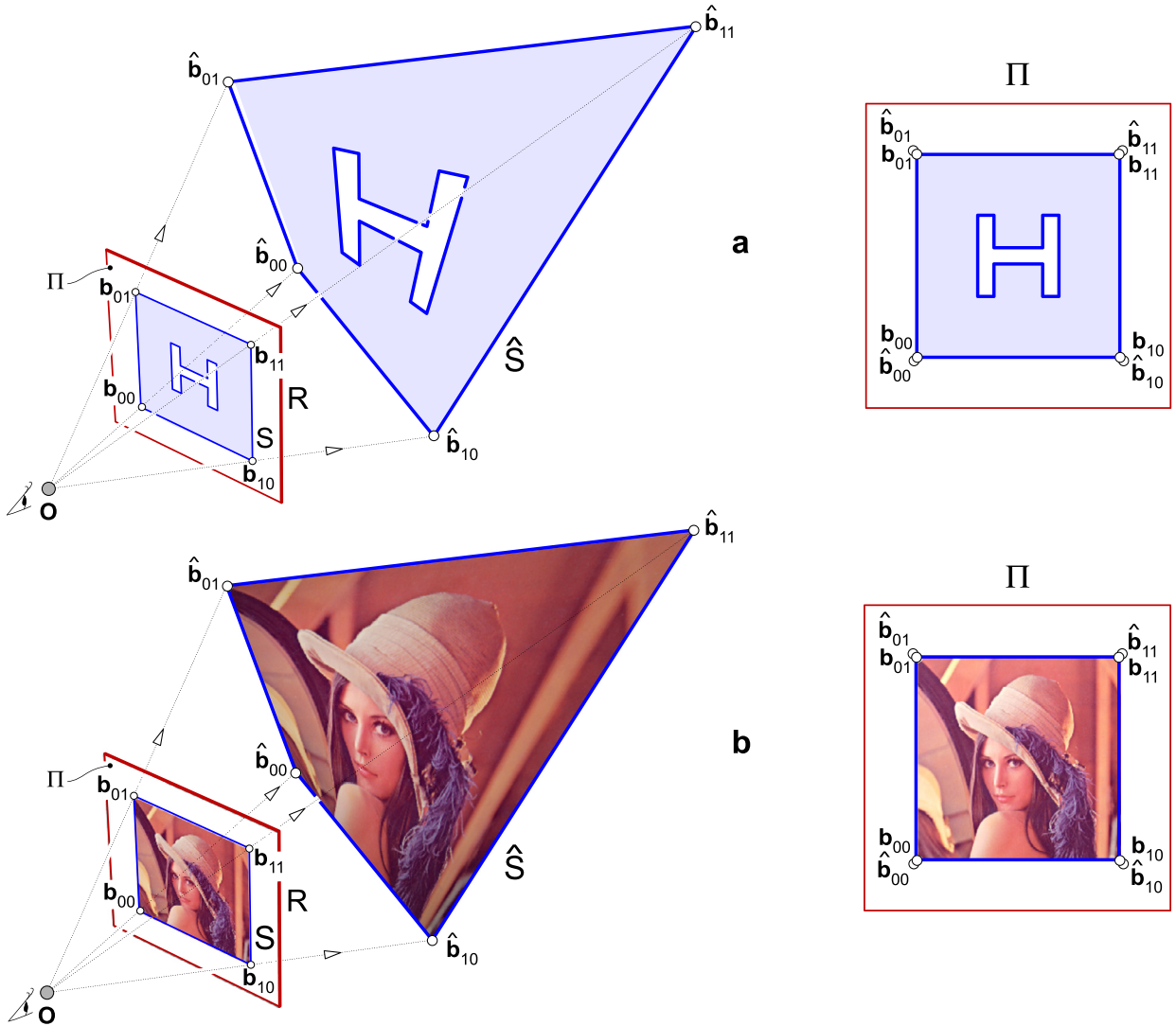


Fig. 7. Rational bilinear AFFD using a Bézier rectangle as deformation tool: a) vector image, b) bitmap.

- The origin  $\mathbf{O} = \{0, 0, 0\}^T$  is a *fixed point*, because  $\hat{\mathbf{O}} = \mathbf{O}$ .
- Any line through  $\mathbf{O}$  is mapped to itself, since any point  $\mathbf{p}$  is dilated, using  $\mathbf{O}$  as center.

#### 4.1. Rational linear case: Bézier form

The simplest volumetric deformation tool is a Bézier tetrahedral volume (Hoschek and Lasser, 1993) of degree  $n = 1$ , with four control points  $\{\mathbf{b}_i\}_{i=0}^3$  corresponding to the vertices of a reference tetrahedron  $T$  (Fig. 8). Similarly to the planar case, these points define, as local parameter space, a system of barycentric coordinates  $\mathbf{u} = (u_0, u_1, u_2, u_3)$ . The four points  $\mathbf{b}_i$  are assigned initially a unit weight, and then the user displaces them along radial directions  $\mathbf{O}\mathbf{b}_i$ , to their final positions  $\hat{\mathbf{b}}_i$ , thus defining the new homogeneous points  $\hat{\mathbf{b}}_i$  (5) and a linear function  $\delta(\mathbf{u})$  (6):

$$\hat{\mathbf{p}} = \left\{ \begin{array}{l} \mathbf{p} \\ \delta(\mathbf{u}) \end{array} \right\}, \quad \delta(\mathbf{u}) = \sum_{i=0}^3 u_i \delta_i. \quad (10)$$

The resulting rational linear AFFD transforms lines to lines, and planes to planes. Therefore, given a faceted  $S$  with planar faces,  $\hat{S}$  remains an object with planar faces.

In fact, the linear AFFD of Section 3.1 can be regarded as the effect of a certain 3D AFFD on the view plane  $\Pi$ : just define a tetrahedron  $T$  whose face  $\mathbf{b}_0\mathbf{b}_1\mathbf{b}_2$  coincides with the triangle on  $\Pi$  of the planar case. Since the remaining point  $\mathbf{b}_3$  exerts not influence on  $\Pi$ , we can choose  $\mathbf{b}_3$  and  $\hat{\mathbf{b}}_3$  arbitrarily, for instance a fixed point  $\mathbf{b}_3 = \hat{\mathbf{b}}_3 = \mathbf{O}$  ( $\delta_3 = 1$ ).



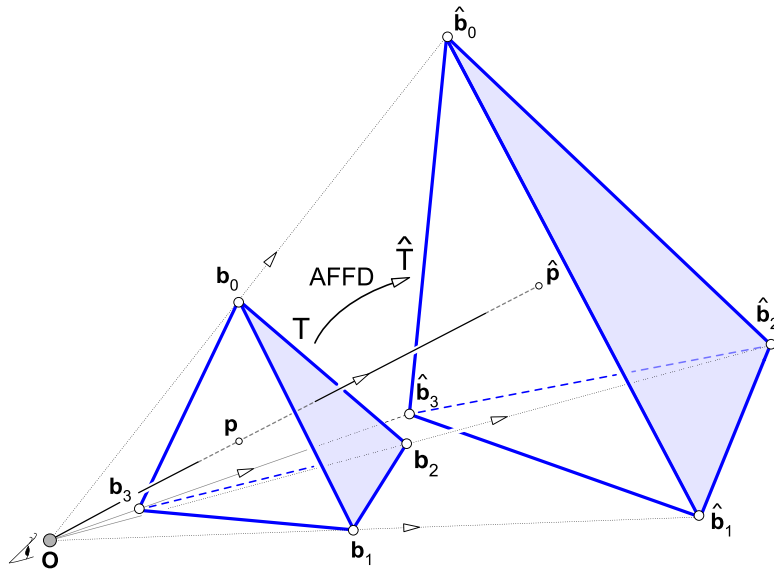


Fig. 8. Bézier tetrahedron as deformation tool in a rational linear AFFD.

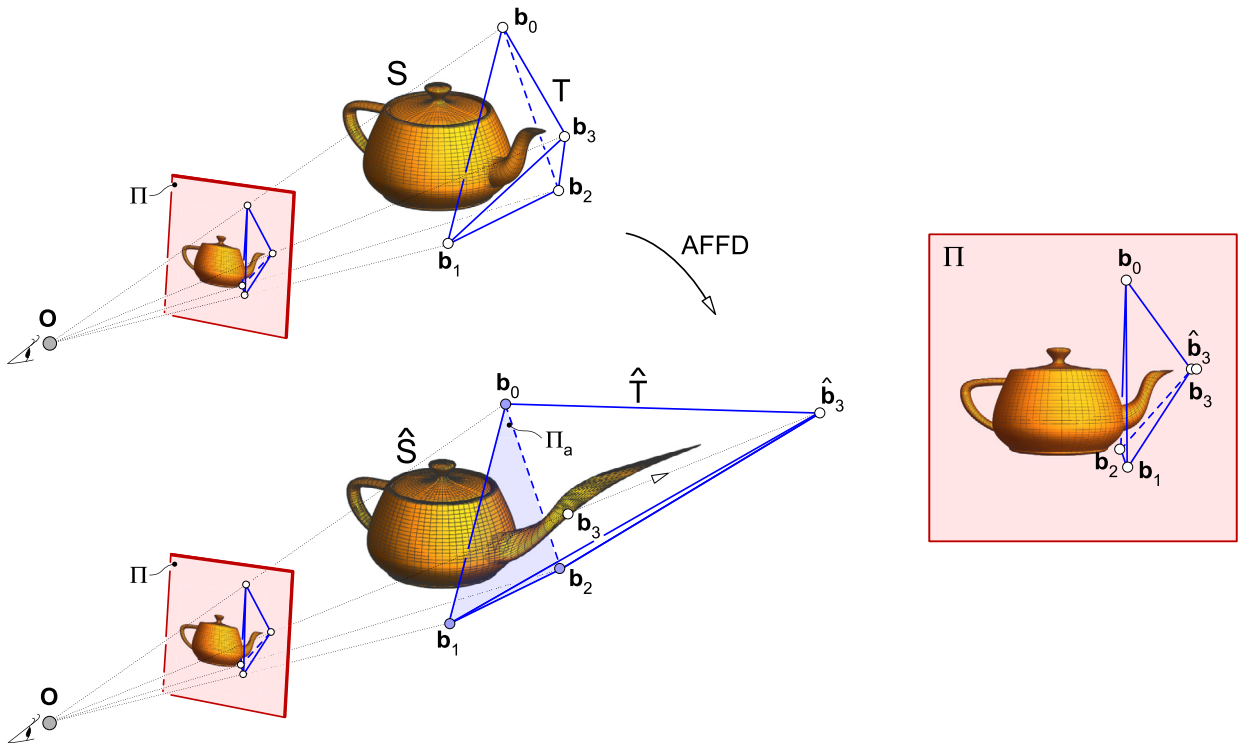


Fig. 9. Rational linear AFFD of the Utah teapot, composed of bicubic Bézier patches.

Analogously to the linear case of Section 3.1, a NURBS transforms to another NURBS of the same degree, with new control points given by (9). For example, in Fig. 9 we have deformed a teapot composed of bicubic Bézier patches. Although a FFD is usually aimed at global deformations, in this case we localized a stretching in the spout  $S$ . Thus, we chose a tetrahedron  $T$  embedding  $S$ , restricting the AFFD to points contained in  $T$  (i.e., with positive barycentric coordinates). To guarantee  $C^0$  continuity in the final teapot and avoid the continuity problems pointed out by Bechmann (1994), the triangular face  $b_0b_1b_2$  where  $T$  intersects the teapot does not move. Therefore, we displace only  $b_3$ , that is:

$$\delta_0 = \delta_1 = \delta_2 = 1, \quad \delta_3 \neq 1. \tag{11}$$

In this case, as an alternative to displacing  $\mathbf{b}_3$ , we could apply instead a point-based deformation (Gain and Bechmann, 2008), by picking an arbitrary point  $\mathbf{p}$  on  $S$ , not contained in the face  $\mathbf{b}_0\mathbf{b}_1\mathbf{b}_2$ , and prescribing its new position  $\hat{\mathbf{p}} = \mathbf{p}/\delta$  along a radial line  $\mathbf{Op}$ . This constraint furnishes the value  $\delta$ . Finally, if  $u_i$  denotes the barycentric coordinates of  $\mathbf{p}$ , taking into account (11) and that  $\sum u_i = 1$ , the required value  $\delta_3$  (and hence  $\hat{\mathbf{b}}_3$ ) is isolated from (10):

$$\hat{\mathbf{b}}_3 = \frac{\mathbf{b}_3}{\delta_3}, \quad \delta_3 = 1 + \frac{\delta - 1}{u_3}.$$

#### 4.2. Rational linear case as a perspective collineation: matrix form

Next, we check that our rational linear AFFD is simply a geometric and intuitive way to construct a *perspective collineation* (Pottmann and Wallner, 2001), in a Bézier fashion. A collineation was also defined by Hansford and Collins (2007), but in a less direct manner. Clearly, the AFFD is a linear map in projective space, mapping this space into itself, and hence a collineation (i.e., it transforms collinear points to collinear points). It remains to check the existence of the two elements characterizing a perspective collineation:

- A fixed point (*center*): We already know that this is the point  $\mathbf{O}$ .
- A fixed *axis plane*  $\Pi_a$ : Since  $\delta(\mathbf{u})$  (10) is linear in terms of barycentric coordinates, it is also linear in affine coordinates (1) of points  $\mathbf{p}$ . Therefore, the implicit equation  $\delta(\mathbf{u}) = 1$  defines a plane  $\Pi_a$ , clearly invariant (unit dilation).

Thus, the function  $\delta(\mathbf{u})$  has a clear geometric meaning, as  $\delta(\mathbf{u}) - 1$  is proportional to the signed distance to  $\Pi_a$ . As an alternative to the sum (10),  $\delta(\mathbf{u})$  can be rewritten in terms of a scalar product:

$$\delta(\mathbf{u}(\mathbf{p})) = \mathbf{p} \cdot \mathbf{d} + d, \quad \mathbf{d} = \{d_0, d_1, d_2\}^T, \tag{12}$$

where  $\mathbf{d}$  denotes a vector normal to  $\Pi_a$ , and  $d$  a certain scalar. To find  $\mathbf{d}, d$ , consider the affine points:

$$\mathbf{e}_0 = \begin{Bmatrix} 1 \\ 0 \\ 0 \end{Bmatrix}, \quad \mathbf{e}_1 = \begin{Bmatrix} 0 \\ 1 \\ 0 \end{Bmatrix}, \quad \mathbf{e}_2 = \begin{Bmatrix} 0 \\ 0 \\ 1 \end{Bmatrix}, \quad \mathbf{O} = \begin{Bmatrix} 0 \\ 0 \\ 0 \end{Bmatrix},$$

compute their barycentric coordinates  $\mathbf{u}$  (some may be negative) and isolate from (12):

$$d_i = \delta(\mathbf{u}(\mathbf{e}_i)) - d, \quad d = \delta(\mathbf{u}(\mathbf{O})). \tag{13}$$

Once these values  $\mathbf{d}, d$  are determined, expression (12) does not require the computation of the barycentric coordinates of a given point  $\mathbf{p}$ , so it is more efficient than the sum in (10). Therefore, we recommend the use of (12) when deforming a polygonal object with a large number of vertices.

Given the center  $\mathbf{O}$ , the collineation is thus defined by only 4 parameters, namely  $\mathbf{d}$  and  $d$  (13). In contrast, the general Bézier construction in the previous section requires as input four initial points and their displacements. We conclude that a given collineation can be reproduced with different Bézier constructions. Nevertheless, this redundancy is convenient for the user, who can control in a more intuitive manner the deformation within an arbitrary region  $T$  of interest.

To set the axis plane  $\Pi_a$  using the Bézier construction, simply choose three control points on  $\Pi_a$  (for instance,  $\mathbf{b}_0, \mathbf{b}_1, \mathbf{b}_2$  as in the example of Fig. 9) and do not move them. The remaining fourth degree of freedom available in a perspective collineation is controlled by the radial displacement of the remaining point  $\mathbf{b}_3$ . Alternatively, we could set this point at the origin ( $\mathbf{b}_3 = \mathbf{O}$ ) and then apply (5), which in this case amounts to changing its weight (without displacement). Thus, all vertices of the tetrahedron  $T$  are fixed and the interior of  $T$  is mapped to itself by the AFFD.

Finally, the collineation admits a customary homogeneous form, in terms of a  $4 \times 4$  matrix  $M$ :

$$\hat{\mathbf{p}} = \Phi(\mathbf{p}) = M\mathbf{p}. \tag{14}$$

Since this expression for the AFFD coincides with (10), and taking into account (12), the matrix  $M$  (14) enjoys a simple structure:

$$M = \begin{bmatrix} I & 0 \\ \mathbf{d} & d \end{bmatrix},$$

where  $I$  denotes a  $3 \times 3$  identity matrix, and  $\mathbf{d}, d$  are given by (13).

#### 4.3. Quadratic and higher-degree AFFD

The extension to an AFFD of higher degree is a straightforward exercise. In particular, with a quadratic (degree  $n = 2$ ) tetrahedral Bézier volume as deformation tool, at each plane we reproduce the quadratic construction of Section 3.2 (i.e., an inverse of a stereographic projection), so that planes transform to quadrics through  $\mathbf{O}$ .

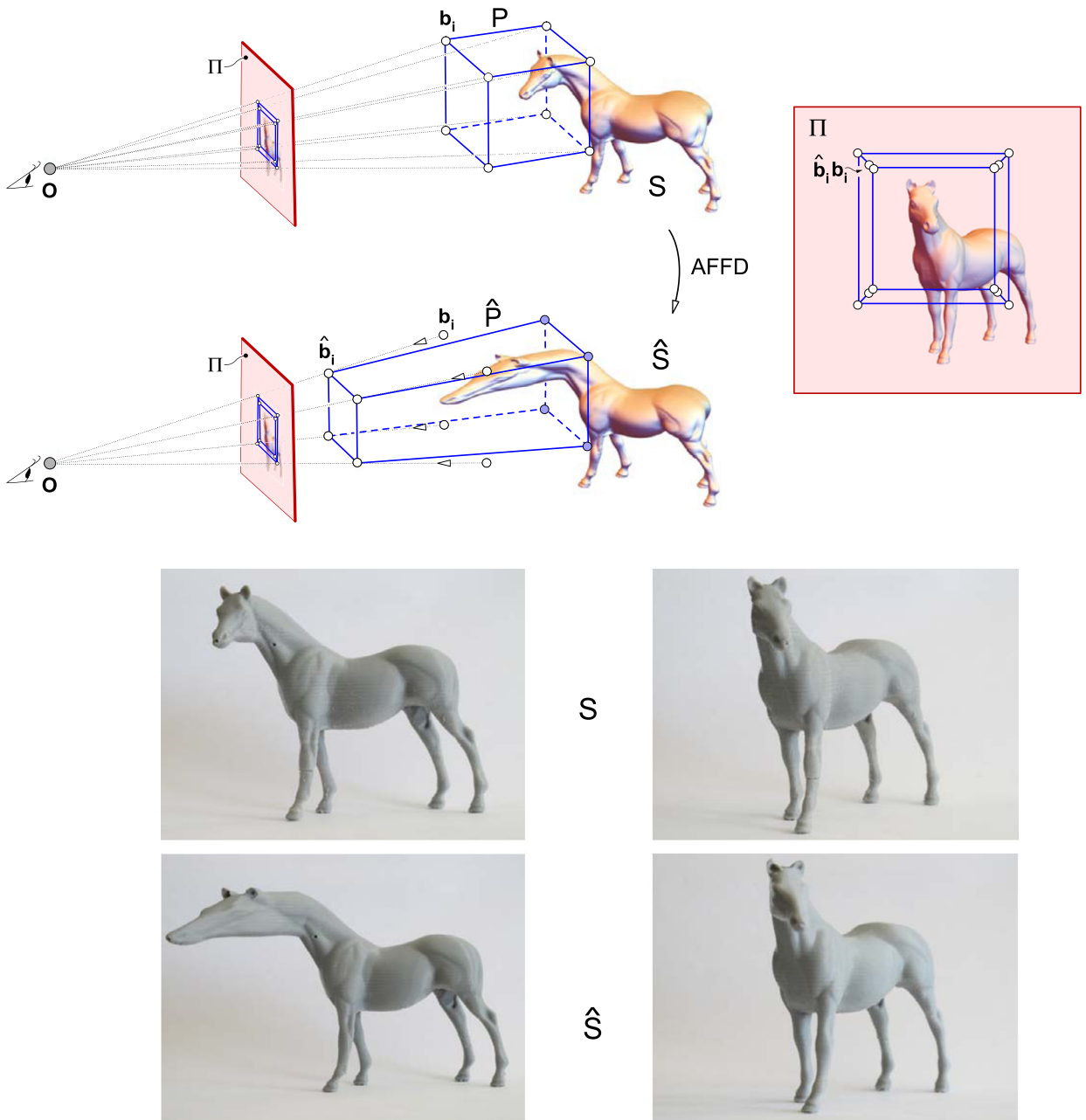


**Fig. 10.** Rational trilinear AFFD of a polygonal model  $S$ , using a Bézier cube as deformation tool. 3D-printed objects  $S$ ,  $\hat{S}$  and their projections.

Instead of a Bézier tetrahedron, we can employ a parallelepiped  $P$  as deformation tool, i.e., a trivariate tensor-product Bézier volume in rational version (Kalra et al., 1992; Davis and Burton, 1991; Lasser, 1994). Now, the user defines the reference  $P$  embedding the object, and then chooses the degree of the deformation tool. For a Bézier tool, this means a regular control grid, resulting from degree-elevating a trilinear hyperpatch. Therefore, the embedding function  $\mathbf{E}$  (4) amounts to an affine transformation, mapping  $P$  to a unit cube, associated to the local parameter space  $\mathbf{u} = (u, v, w) \in [0, 1] \times [0, 1] \times [0, 1]$ . These control points, initially with unit weights, are displaced anamorphy (5) to define a rational hyperpatch  $\mathbf{h}(\mathbf{u})$ .

An example is shown in Fig. 10, where we deformed a polygonal model of a horse (Turk and Mullins, 1999) with a simple Bézier cuboid of degree  $(1, 1, 1)$ , defined by eight control points corresponding to the vertices of  $P$ . This geometry yields a rational trilinear hyperpatch, the rational version of the deformation tool described by Pottmann et al. (2007). Similarly to the teapot of Fig. 9, to guarantee  $C^0$  continuity in a local deformation we do not move the control points on the face of  $P$  intersecting the model (Sederberg and Parry, 1986). Note also that the initial cuboid  $P$  and its anamorphic image  $\hat{P}$  share a common projection on  $\Pi$ , so an observer at  $\mathbf{O}$  would easily mistake  $\hat{P}$  for the more familiar cuboid  $P$ ,

with rectangular faces at right angles to each other. This is the precisely the effect involved in the celebrated *Ames room* (IllusionWorks, 1997) used to create optical illusions.

The initial horse  $S$  and its anamorphic version  $\hat{S}$  have been 3D-printed, to check the anamorphosis. The model  $\hat{S}$  contains a slender through hole, materializing a ray fired from the viewpoint  $\mathbf{O}$ , to help the viewer orient  $\hat{S}$  correctly. To visualize the anamorphosis, the viewer holds  $\hat{S}$  at a prescribed distance and aligns it so that the hole is seen through. To avoid any clues from *stereopsis* (i.e., the depth perception resulting from by binocular vision),  $\hat{S}$  must be viewed with only one eye.

Clearly, we could use any control-point based deformation tool in its rational form, including pentahedral Bézier volumes (Hoschek and Lasser, 1993), NURBS volumes (Lamoussin and Waggenspack, 1994), or even weighted T-spline volumes (Song and Yang, 2005), the volumetric generalization of T-splines (Sederberg et al., 2003). A higher degree of the deformation tool allows a higher continuity of  $\hat{S}$  when  $S$  is only partially contained in the initial volume, by selectively displacing its control points. We could also achieve a continuous deformation by piecing several Bézier tetrahedra, rather than using just one, following the idea of the CFFD (Continuous Free-Form Deformation) proposed by Bechmann et al. (1997).

## 5. Conclusions

We have developed a simple, yet powerful method to create a digital anamorphosis, called AFFD (Anamorphic Free-Form Deformation), by endowing a rational FFD with an anamorphic character. The key idea is the use of homogeneous coordinates with origin at the viewpoint where the observer is located. In this setting, the problem becomes trivial, because to displace a certain point anamorphically (along a radial direction passing through the viewpoint), we only alter its last homogeneous coordinate.

Instead of displacing an object point by point, we can displace in the same manner the NURBS control points of an object defined by NURBS curves or patches. In the case of a complex geometry, the AFFD provides a more convenient alternative to generate an anamorphic version. We embed the (planar or 3D) object in a (planar or 3D) structure and then deform the structure by applying an anamorphic transformation to the control points of the lattice. The user moves the control points along radial lines through the viewpoint to the desired final position, whereas the weights, inversely proportional to the distance to the viewpoint, come as a byproduct. Remarkable cases are the AFFD of a planar object with a rational linear Bézier triangle (resulting in a projection into another plane) or with a rational quadratic Bézier surface (corresponding to the inverse of a stereographic projection from a quadric). In case of a rational linear Bézier tetrahedron as deformation tool, the volumetric AFFD is nothing else than a perspective collineation, defined geometrically in a Bézier fashion.

The AFFD gives a notable example where the rational model provides a clear advantage over its polynomial counterpart, as anticipated in any topic related to realistic perspective maps (Farin, 1989). Notwithstanding that the rational form introduces an unnecessary complication in certain constructions (Piegl et al., 2014), in the AFFD it is fully justified. Although the mathematical underpinnings involve homogeneous coordinates and projective space, the user input amounts to displacing affine points in Euclidean space. Thus, we avoid altogether a nuisance of the rational model pointed out by Farin (1992), namely having to choose the weights.

Our AFFD admits a simple explicit expression, so it is not restricted to polygonal objects and can also be applied in native form to those defined by parametric curves and surfaces. In particular, an AFFD applied to a NURBS yields a NURBS; formally speaking, the set of NURBS is closed with respect to the AFFD. In the simple rational linear case, the degree is unchanged, and the new points and weights are trivially computed. When the deformation tool is not rational linear, the exact NURBS representation implies polynomial composition and hence a high final degree, which may not be transferable to many commercial systems, not admitting such high degrees. This problem is inherent to any polynomial/rational FFD scheme when the precise explicit representation of output is required. A possible solution (Sánchez-Reyes and Chacón, 2012) would be to generate a low-degree Hermite approximation of the resulting high-degree curve or patch, by truncating its expansion in a modified Newton form (Sánchez-Reyes, 2000; Sánchez-Reyes and Chacón, 2005).

The extension to EFFF (Extended Free-Form Deformation) (Coquillart, 1990) seems also feasible. The EFFF has an added complexity, namely that the embedding function is no longer a simple affine transformation. However, this becomes immaterial, because the key step to generate an anamorphosis is the deformation, where we simply have to change the last homogeneous coordinate of the lattice control points.

## Acknowledgements

This research was supported by the Spanish *Ministerio de Economía y Competitividad* (Plan Estatal de Investigación Científica Técnica y de Innovación), under research grants DPI2012-32278 and DPI2015-65472-R, co-financed by the ERDF (European Regional Development Fund). We are grateful to Dr. M.A. Caminero for his assistance in taking the pictures of Fig. 10, and to the referees for their suggestions, which improved the quality of this article.

## References

- Bechmann, D., 1994. Space deformation models survey. *Comput. Graph.* 18 (4), 571–586.
- Bechmann, D., Bertrand, Y., Thery, S., 1997. Continuous free-form deformation. *Comput. Netw. ISDN Syst.* 29 (14), 1715–1725.
- Beever, D., 2012. Pavement drawings – 3D illusions. <http://www.julianbeever.net>.
- Bian, Z., Hu, S.-H., 2011. Preserving detailed features in digital bas-relief making. *Comput. Aided Geom. Des.* 28 (4), 245–256.

- Boehm, W., Hansford, D., 1991. Bézier patches on quadrics. In: Farin, G. (Ed.), *NURBS for Curve and Surface Design*. SIAM, Philadelphia, pp. 1–14.
- Coquillart, S., 1990. Extended free-form deformation: a sculpturing tool for 3D geometric modeling. *Comput. Graph.* 24 (4), 187–196.
- Davis, O.R., Burton, R.P., 1991. Free-form deformation as an interactive modeling tool. *J. Imag. Tech.* 17 (4), 181–187.
- Di Paola, F., Pedone, P., Inzerillo, L., Santagati, C., 2015. Anamorphic projection: analogical/digital algorithms. *Nexus Netw. J.* 17 (1), 253–285.
- Elber, G., 2011. Modeling (seemingly) impossible models. *Comput. Graph.* 35, 632–638.
- Farin, G., 1989. Rational curves and surfaces. In: Lyche, T., Schumaker, L.L. (Eds.), *Mathematical Methods in Computer Aided Geometric Design*. Academic Press, pp. 215–238.
- Farin, G., 1992. From conics to NURBS: a tutorial and survey. *IEEE Comput. Graph. Appl.* 12 (5), 78–86.
- Farin, G., 1999. *NURBS: From Projective Geometry to Practical Use*, 2nd ed. AK Peters.
- Farin, G., 2002. *Curves and Surfaces for Computer Aided Geometric Design*, 5th ed. Morgan Kaufmann.
- Farin, G., Hansford, D., 2000. *The Essentials of CAGD*. AK Peters.
- FDG Entertainment GmbH & Co., 2015. *Blueprint 3D*. <http://www.fdg-entertainment.com/en/iPhone-Games/Blueprint-3D-iPhone.html>.
- Gain, J., Bechmann, D., 2008. A survey of spatial deformation from a user-centered perspective. *ACM Trans. Graph.* 27 (4), 107:1–107:21.
- Hansford, D., Collins, D., 2007. Anamorphic 3D geometry. *Computing* 79, 211–223.
- Hoschek, J., Lasser, D., 1993. *Fundamentals of Computer Aided Geometric Design*. AK Peters.
- IllusionWorks, 1997. *Ames Room*. [http://psylux.psych.tu-dresden.de/i1/kaw/diverses%20Material/www.illusionworks.com/html/ames\\_room.html](http://psylux.psych.tu-dresden.de/i1/kaw/diverses%20Material/www.illusionworks.com/html/ames_room.html).
- Kalra, P., Mangili, A., Thalmann, N.M., Thalmann, D., 1992. Simulation of facial muscle actions based on rational free form deformations. *Comput. Graph. Forum* 11 (3), 59–69.
- Kent, P., 2013. *Art of anamorphosis*. <http://www.anamorphosis.com>.
- Kerber, J., Wang, M., Chang, J., Zhang, J.J., Belyaev, A., Seidel, H.P., 2012. Computer assisted relief generation—a survey. *Comput. Graph. Forum* 31 (8), 2363–2377.
- Lamoussin, H.J., Waggenspack, W.N., 1994. NURBS-based free-form deformations. *IEEE Comput. Graph. Appl.* 14 (6), 59–65.
- Lasser, D., 1994. Rational tensor product Bézier volumes. *Comput. Math. Appl.* 28 (8), 49–62.
- Lodha, S., Warren, J., 1990. Bézier representation for quadric surface patches. *Comput. Aided Des.* 22 (9), 574–579.
- National Geographic Channel, 2015. *Brain games: seeing is believing*. <http://channel.nationalgeographic.com/brain-games/videos/brain-games-seeing-is-believing-preview/>.
- Piegl, L.A., Tiller, W., 1997. *The NURBS Book*, 2nd ed. Springer.
- Piegl, L.A., Tiller, W., Rajab, K., 2014. It is time to drop the “R” from NURBS. *Eng. Comput.* 30 (4), 703–714.
- Pottmann, H., Wallner, J., 2001. *Computational Line Geometry*. Springer.
- Pottmann, H., Asperl, A., Hofer, M., Kilian, A., 2007. *Architectural Geometry*. Bentley Institute Press, Exton, PA, USA.
- Ravnik, R., Batagelj, B., Kverh, B., Solina, F., 2014. Dynamic anamorphosis as a special, computer-generated user interface. *Interact. Comput.* 26 (1), 46–62.
- Salomon, G., 2006. *Transformations and Projections in Computer Graphics*. Springer.
- Salomon, G., 2011. *The Computer Graphics Manual*, vol. 2. Springer.
- Sánchez-Reyes, J., 1997. A simple technique for NURBS shape modification. *IEEE Comput. Graph. Appl.* 17 (1), 52–59.
- Sánchez-Reyes, J., 2000. Applications of the s-power basis in geometry processing. *ACM Trans. Graph.* 9 (1), 27–55.
- Sánchez-Reyes, J., Chacón, J.M., 2005. s-power series: an alternative to Poisson expansions for representing analytic functions. *Comput. Aided Geom. Des.* 22 (2), 103–119.
- Sánchez-Reyes, J., Chacón, J.M., 2012. Hermite approximation for free-form deformation of curves and surfaces. *Comput. Aided Des.* 44 (5), 445–456.
- Sánchez-Reyes, J., Paluszny, M., 2000. Weighted radial displacement: a geometric look at Bézier conics and quadrics. *Comput. Aided Geom. Des.* 17 (3), 267–289.
- Schüller, C., Panozzo, D., Sorkine-Hornung, O., 2014. Appearance-mimicking surfaces. *ACM Trans. Graph.* 33 (6), 216:1–10.
- Sederberg, T.W., Anderson, D.C., 1985. Steiner surface patches. *IEEE Comput. Graph. Appl.* 5 (5), 23–36.
- Sederberg, T.W., Parry, S.R., 1986. Free-form deformation of solid geometric models. *Comput. Graph.* 20 (4), 151–196.
- Sederberg, T.W., Zheng, J., Bakenov, A., Nasri, A., 2003. T-splines and T-NURCCs. *ACM Trans. Graph.* 22 (3), 477–484.
- Sela, G., Elber, G., 2007. Generation of view dependent models using free form deformation. *Vis. Comput.* 23 (3), 219–229.
- Stanford Computer Graphics Laboratory, 2014. *The Stanford 3D Scanning Repository*. <http://graphics.stanford.edu/data/3Dscanrep/>.
- Song, W., Yang, X., 2005. Free-form deformation with weighted T-spline. *Vis. Comput.* 21 (3), 139–151.
- Teller, S.J., Séquin, C., 1991. Constructing easily invertible Bézier surfaces that parametrize general quadrics. In: Rossignac, J., Turner, J. (Eds.), *Proceedings Symposium on Solid Modeling Foundations and CAD/CAM Applications*. ACM Press, New York.
- Topper, D., 2000. On anamorphosis: setting some things straight. *Leonardo* 33 (2), 115–124.
- Turk, G., Mullins, B., 1999. *Georgia Institute of Technology, Large Geometric Models Archive*. [http://www.cc.gatech.edu/projects/large\\_models/horse.html](http://www.cc.gatech.edu/projects/large_models/horse.html).